



# Antibacterial Properties and Cytotoxicity of 100% Waste Derived Alkali Activated Materials: Slags and Stone Wool-Based Binders

Caterina Sgarlata<sup>1†</sup>, Giovanni Dal Poggetto<sup>1†</sup>, Federica Piccolo<sup>1†</sup>, Michelina Catauro<sup>2</sup>, Katja Traven<sup>3</sup>, Mark Češnovar<sup>3</sup>, Hoang Nguyen<sup>4</sup>, Juho Yliniemi<sup>4</sup>, Luisa Barbieri<sup>1</sup>, Vilma Ducman<sup>3</sup>, Isabella Lancellotti<sup>1</sup> and Cristina Leonelli<sup>1\*</sup>

<sup>1</sup>Department of Engineering “Enzo Ferrari”, University of Modena and Reggio Emilia, Modena, Italy, <sup>2</sup>Department of Engineering, University of Campania “Luigi Vanvitelli”, Aversa, Italy, <sup>3</sup>Slovenian National Building and Civil Engineering Institute-ZAG, Ljubljana, Slovenia, <sup>4</sup>Fibre and Particle Engineering Research Unit, University of Oulu, Oulu, Finland

## OPEN ACCESS

### Edited by:

Brant Walkley,  
The University of Sheffield,  
United Kingdom

### Reviewed by:

João Castro-Gomes,  
University of Beira Interior, Portugal  
Neven Ukrainczyk,  
Darmstadt University of Technology,  
Germany

### \*Correspondence:

Cristina Leonelli  
cristina.leonelli@unimore.it

†These authors have contributed  
equally to this work and share  
first authorship

### Specialty section:

This article was submitted to  
Structural Materials,  
a section of the journal  
Frontiers in Materials

Received: 31 March 2021

Accepted: 10 June 2021

Published: 15 July 2021

### Citation:

Sgarlata C, Dal Poggetto G, Piccolo F,  
Catauro M, Traven K, Češnovar M,  
Nguyen H, Yliniemi J, Barbieri L,  
Ducman V, Lancellotti I and Leonelli C  
(2021) Antibacterial Properties and  
Cytotoxicity of 100% Waste Derived  
Alkali Activated Materials: Slags and  
Stone Wool-Based Binders.  
Front. Mater. 8:689290.  
doi: 10.3389/fmats.2021.689290

In this study we compare the leaching behavior and the antibacterial and cytotoxic properties of 100% slag or stone wool derived alkali activated materials. The antibacterial activity was measured as the inhibiting capacity against two Gram-negative bacterial strains, *Escherichia coli* and *Pseudomonas aeruginosa* and one Gram-positive bacterial strain: *Enterococcus faecalis*. The cytotoxicity properties were tested on mouse embryonic fibroblast NIH-3T3 cell-line. It was proved that the high quality of the 3D aluminosilicate network of the consolidated materials obtained from powders of CaO or MgO-rich slags or stone wool, opportunely activated with NaO and/or Na-silicate, was capable of stabilizing heavy metal cations. The concentrations of leachate heavy cations were lower than the European law limit when tested in water. The effect of additives in the composites, basal fibers or nanocellulose, did not reduce the chemical stability and slightly influenced the compressive strength. Weight loss in water increased by 20% with basalt fibers addition, while it remained almost constant when nanocellulose was added. All the consolidated materials, cement-like in appearance, exhibited limited antibacterial properties (viability from 50 to 80% depending on the bacterial colony and the amount of sample) and absence of cytotoxicity, envisaging good acceptance from part of the final consumer and zero ecological impact. CaO-rich formulations can replace ordinary Portland cement (showing bacterial viability at 100%) with a certain capability for preventing the reproduction of the *E. coli* and *S. aureus* bacteria with health and environmental protection results.

**Keywords:** antibacterial properties, cytotoxicity, alkali-activated materials, slag, stone wool, waste utilization, social acceptance

## INTRODUCTION

Reducing inorganic waste and recycling them in the production of common construction building materials has become a global challenge with a view to a circular economy and sustainable construction. On the one hand, for the circular economy, it is essential to recycle materials from waste in order “to close the loop”. On the other hand, sustainable design and construction requires

creating structures and using environmentally friendly and resource-efficient processes throughout the life cycle of a building. The inert inorganic wastes are a subgroup that might not encounter specific difficulties, but even non-technical aspects such as psychosocial impacts and social acceptance need to rely increasingly on safe products and processes and by informing citizens and civil society organizations.

The economic impacts of the product obtained with a large amount of industrial by-products or inert inorganic waste should help fight this problem, when proper communication is actuated.

The involvement of stakeholders with different backgrounds is a key enabler of the process. As in the EU project FLOW “Lightweight alkali activated composite foams based on secondary raw materials”<sup>1</sup> were inert waste producers, metallurgical slags from Slovenia and Finland as well as end-of-life stone wool (i.e., material in the insulating panels) from Finland have been involved in the design and realization of the insulating panels, composites and mortars for sustainable building materials.

In particular, the large amount of slags from the metallurgical process are still under-utilized. Unlike blast furnace slag from iron-making process, which has been already commercialized and should be reserved to use as a supplementary cementitious material in the cement industry, other slags particularly from steel-making processes need suitable solutions for their characteristics. Basic oxygen furnace (BOF) slag and desulfurization furnace (De-S) slag are often suffering with a high free-CaO content which will lead to dimension instability of hardened concrete due to the late reaction of f-CaO (Jiang et al., 2018). Hence, the recycling rate is currently relatively low (i.e., mainly in some soil stabilization), and the availability of these steel slags is abundant to consider their utilization and application in the construction industry. Therefore, research work that can enable the use of steel slags and overcome their obstacles is of interest.

Similarly to other cementitious materials, AAMs exhibit brittle failure when it comes to fracture behavior. To reduce this sudden failure, fibrous reinforcement is known as one of the best options to improve the ductility of AAMs. However, it is unclear whether these fibers will react in the alkaline activation, change the reaction products, and eventually alter the antibacterial properties and cytotoxicity of the developed AAMs reported here. Hence, we investigated the contribution of both inorganic (i.e., basalt fiber in one mix) and organic (i.e., cellulose fiber in a second mix) to the antibacterial properties and cytotoxicity of these fiber-reinforced composites in comparison to the plain slag-based material.

An additional aspect lies in the fragility of territories where the accumulation of these slags is present. In the cases of Slovenia, due to the limited national surface, and in Finland, due to the harsh climate conditions, the problems generated by unwise use of by-products, industrial inert wastes, and construction and demolition waste (C&DW), require a strong activity of engineers and social designer aimed to the efficient proposal/design/realization of waste-derived proved or close-loop recycling.

Regarding stone wool (a waste from building insulation materials commonly used in Northern Europe), the material is considered as waste in many places due to its low-rate utilization. More than two million tons of mineral wool is generated each year in Europe and this number is also expected to increase over time (Väntsi and Kärki, 2014). Therefore, using stone wool as a precursor to produce cementitious binder can facilitate the principles of circular economy and close the loop for this industrial waste. The stone wool has been proven its potential to use as a precursor for alkali-activated material (Yliniemi et al., 2016; Kinnunen et al., 2017; Yliniemi et al., 2020). However, the performance of alkali-activated stone wool in terms of antibacterial properties and cytotoxicity remains unknown. Therefore, there is a need to shed light on this aspect of the binder prior to its use as a building material.

Taking into account the few previous studies on the antibacterial and/or cytotoxicity aspects of geopolymers (Catauro et al., 2017; Rubio-Avalos, 2018; Catauro et al., 2021) and those related to their ability to adsorb bacterial protein, protein toxins, bacteria and eventually antibiotics in their engineered macroporous, and mesoporous (Popovich et al., 2020) we measured the antibacterial activity as the inhibiting capacity against two Gram-negative bacterial strains, *Escherichia coli* and *Pseudomonas aeruginosa* and one Gram-positive bacterial strain: *Enterococcus faecalis*. The cytotoxicity properties were tested on mouse embryonic fibroblast NIH-3T3 cell-line. No specific additives were used in the formulations to increase their natural and intrinsic antibacterial properties, differently from what proposed in literature (Rubio-Avalos, 2018).

The present study focuses contemporary on these two aspects, combining the social design of new building products formulated on 100 wt% metallurgical slags and 100% stone wool from C&DW and the investigation of bioenvironmental impact. The final output is the presentation of a safe and performant product fully characterized in terms of leaching of heavy metals, antibacterial properties, cytotoxicity yet fulfilling the regulation requirements for mechanical performance and durability (freeze-thaw cycling). The leaching behavior was tested accordingly to European standard EN 12457, and the release in water of heavy metals cation as the change of pH of the solution was related to the viability of Gram-positive and Gram-negative bacteria as well as murine fibroblast living cells line.

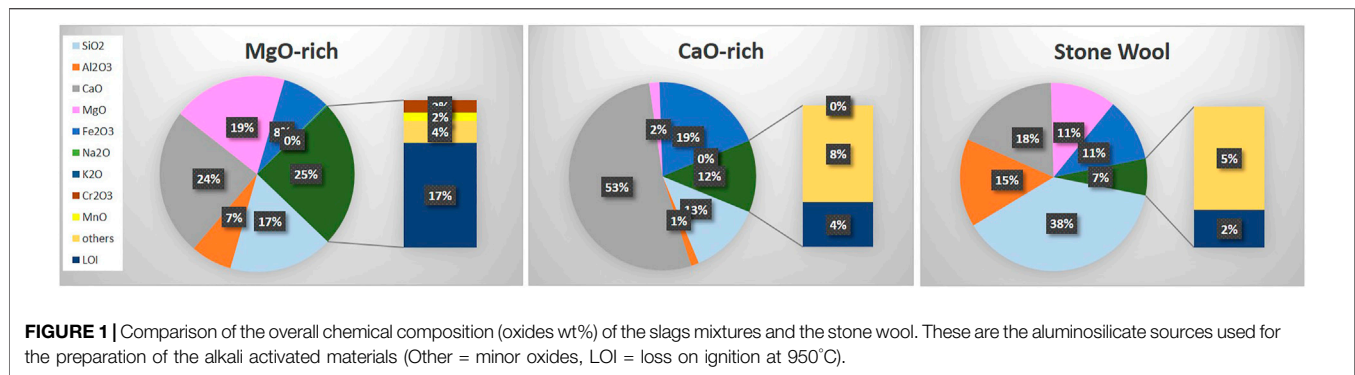
## MATERIALS AND METHODS

### Starting Materials and Powder Mixtures

The aluminosilicate sources for the preparation of the alkali activated materials are MgO-rich slags, CaO-rich slags, and stone wool. All these three starting materials were classified as inert wastes (European Waste Code 01 01 01, slags; EWC 17 06 04, insulation materials other than those mentioned in 17 06 01 and 17 06,03<sup>2</sup>). The optimized mix of the slags was presented in previous works, as detailed hereafter.

<sup>1</sup>ERA-MIN2, «FLOW–Lightweight alkali activated composite foams based on secondary raw materials » Project No. C 3330-18-252010, <http://flow.zag.si/en>.

<sup>2</sup><https://www.epa.ie/pubs/reports/waste/stats/wasteclassification/2019%20%20FULL%20template.pdf>



The chemical analysis (via XRF) of the two MgO-rich slags is presented in **Supplementary Table S1 (Supplementary Table S1)**. Electric arc furnace slag, indicated as Slag A, is produced during the manufacture of crude steel by the electric arc furnace (EAF) process<sup>3</sup>. The ladle furnace basic slag, indicated as Slag R, is produced in the secondary refining stage when the steel is desulfurized in the transport ladle (Setién et al., 2009). Both slags were supplied by Slovenians steel-manufacturing companies. The optimized mix of these slags has been presented elsewhere (Češnovar, et al., 2019a) and was defined as the A and R slags with mixture ratios A/R = 1/1 (overall chemical composition is shown in **Figure 1**), with the 90% of the grain size minor than 28.7 and 24.8  $\mu\text{m}$  (C90 value), for Slag A and Slag R, respectively, (Češnovar et al., 2019b).

As far as the CaO-rich slags are concerned, they were both supplied by SSAB Europe Oy (Finland). **Supplementary Table S2** in Supplementary Materials shows the chemical composition of the slags analyzed by X-ray fluorescence spectroscopy (XRF) (PANalytical Omnia Axiosmax). De-S slag was used as a precursor to form the binder, while BOF slag was carbonated to use as aggregates. Prior to its use, the De-S slag was ground and sieved to achieve a maximum particle size of less than 0.1 mm. BOF slag was carbonated at ambient pressure in an environmental chamber with 5%  $\text{CO}_2$  gas flow, a temperature of 23°C, and relative humidity of 60% for 48 h. The overall chemical composition of the final mixture of De-S/BOF = 1/3 is shown in **Figure 1**.

The third kind of aluminosilicate source was used for this study, again we chose a waste-based material: the stone wool from Paroc Group Oy (Finland). Its chemical composition is shown in Supplementary Materials, **Supplementary Table S2** and in **Figure 1**. The wool was milled to reach a median particle size of ca. 10  $\mu\text{m}$  measured by the laser diffraction method with the Fraunhofer model. To activate the stone wool, we used the same alkali solution as used in alkali-activated steel slag.

The MgO-rich slags mixture was activated with sodium silicate Crystal 0112 with 2:1 of  $\text{SiO}_2/\text{Na}_2\text{O}$  (Tennants Distribution Limited, United Kingdom). The alkaline activator for the CaO-rich slag consists of  $\text{Na}_2\text{SiO}_3$  (supplied by Merck KGaA, Germany) and NaOH (8 M) prepared with a silica modulus of

2.5 as optimized in our previous study (Mastali et al., 2020). The alkali solution was prepared and cooled down to room temperature prior to its use.

To improve the mechanical properties and performance of the developed mixes, basalt and cellulose fibers were employed as reinforcement in which **Supplementary Table S3 (Supplementary Materials)** shows the fibers' physical properties. The use of basalt and cellulose fibers were found increasing the mechanical properties of reinforced mixture as reported previously by Mastali et al. (2020). In the present work, the dosage and properties of fibers were used as optimized in the previous work (Mastali et al., 2020).

## Preparation of Alkali Activated Materials (AAMs)

Each formulation of the three different types of wastes was optimized in previous works, as detailed hereafter. In this study we chose to investigate the AAMs binder formulations which provided the highest mechanical performances, plus two of their composites, one with cellulose fiber and one with basalt fibers.

The A and R slags with mixture ratios A/R: 1/1 were activated with sodium silicate with the activator/slag ratio of 0.5 and the amount of sodium silicate 33.3 wt% resulting in sample designated as GP-MgO-rich and already developed and investigated by Češnovar et al. (Češnovar et al., 2019a). Soon after molding the fresh paste into two forms: 1) small disks 5–6 mm in diameter and 3 mm in thickness (for the cytotoxicity test) and 2) 20 × 20 × 80 mm<sup>3</sup> prisms (for the mechanical strength measurements), the mixture was cured in a heat-chamber for 3 days at 70°C to develop suitable mechanical strength. The resulting flexural and compressive strengths at an age of 7 days after molding were 10.6 and 45.0 MPa, respectively. The 3 days curing time might seem as a short curing time for the alkali-activated materials, but for the MgO-rich slags we have already studied the influence of curing on mechanical properties in a previous study (Češnovar et al., 2019b). Within this study we have concluded that specimens cured at 70°C for 3 days attained almost identical (bending as well as compressive) strength to those cured at room temperature for 28 days.

The mixes for alkali-activated steel slags are shown in **Table 1**, and are indicated as GP-CaO-rich. The De-S slag and BOF aggregates were dry mixed together in 2 min. The alkaline

<sup>3</sup><http://www.euroslag.com/products/eaf/>.

**TABLE 1** | Alkali activated materials formulations expressed as weight %.

Mix label	Slag mix (wt%)	Alkali/binder ratio	Fiber (wt%)
GP-MgO-rich	66.6	0.5	None
GP-CaO-rich	50.0	1.0	None
GP-CaO-rich-NC	48.0	1.0	4
GP-CaO-rich-BAS	48.0	1.0	4
GP-SW	71.4	0.4	None

activator was added to the dry mixture and stirred for ca. 2 min. After attaining a homogenous mortar, fibers, prepared according to GP-CaO-rich-NC or GP-CaO-rich-BAS as in **Table 1**, were gradually added to the mortar and mixed for another 3 min at a speed of ca. 200 rpm. The mixture was cast in oiled plastic molds and sealed with plastic bags for 24 h. The samples were casted and cured 1 day before demolding. Then they were cured in a sealed plastic bag for further 27 days prior to further analyses.

The mix recipe of alkali-activated stone wool plain material, GP-SW, is also listed in **Table 1**. Paste samples were prepared by mixing dry stone wool with an alkali activator adopting an optimized formulation (Nguyen et al., 2020). The process was done with a Kenwood 5 L mixer at low (100 rpm) and high (200 rpm) speed for 1 min each level. GP-SW mix was casted in plastic cylinder mold with a diameter and height of ca. 25 and 20 mm, respectively. The samples were then kept in an oven at 60°C for 24 h prior to demolding and cured in sealed plastic bags.

## AAMs Characterization

The formation of the 3D aluminosilicate network in the alkaline activated materials is strictly related to its leaching behavior in water (Ly et al., 2007). For fully geopolymerized formulations, as those based on metakaolin, it was concluded that the optimal leach resistant composition of metakaolin-based geopolymers probably lay at a Si/Al molar ratio substantially higher than two (Rowles and O'Connor, 2003). Being aware that in the case of alkali activated slags or alkali activated stone wool, the microstructure is far from having totally reacted grains, instead of measuring the Si/Al ratio, we experimentally determined the integrity of the structure by testing the consolidated formulations in water. The integrity test that we adopted (Kiventerä et al., 2018), indeed, provided a qualitative result in terms of the eventual visible dissolution of samples and quantitative results expressed in terms of weight loss to quantify the amount of dissolved sample. The compactness of the specimens and their geopolymerization degree were carried out by the pH and ionic conductivity measurements of the leachate in stirring conditions. The chemical analysis was combined with the mechanical performance, since the second provides a quantification of the resistance of the samples under the action of external forces and it gave an idea of the use of large-scale material.

## Chemical Resistance Test in Water

### Integrity Test/Weight Loss

Before the integrity test, samples were put in beakers and completely covered by acetone (C<sub>3</sub>H<sub>6</sub>O) in order to remove all the internal water. After 3 h, the samples were removed from the acetone and left at room temperature for 3 h. Then the samples

were again weighted (w<sub>1</sub>) and placed in backers with MilliQ water (1:100 solid-water ratio). After 24 h, the water was removed and the integrity was evaluated by: 1) final pH solution; 2) smoothness; 3) hardness and finger pressure; 4) water transparency. The samples were again put in acetone for further 3 h and then left again for 3 h at room temperature and weighted (w<sub>f</sub>). The weight loss was calculated using the following equation:

$$\text{Weight loss} = \frac{w_1 - w_f}{w_1} \times 100 \quad (1)$$

### pH and Ionic Conductivity Measurements

Bulk samples in the same conditions of the leaching test (sample immersed in MilliQ water (1:10 solid-water ratio) in stirring conditions), were characterized in terms of conductivity and pH measurements with (Crison GLP31 and Crison GLP21, respectively) from the initial time up to 24 h.

### Normed Leaching Test in Water and ICP Analysis

The ability of leaching heavy metals of all samples was carried out according to the European standard EN 12457 "Characterization of waste-leaching-compliance test for leaching of granular waste materials and sludge". This test was chosen in order to evaluate the hazardousness of the materials according to published studies (Benassi et al., 2019) as being indicative of the level of ecotoxicity of the slags. By this procedure the evaluation of the progressive percolation over time is shortened by directly estimating the maximum possible release of elements and compounds, with a wash operated onto the initial solid sample (procedure that has been adopted by the EU regulators to set legal values). Samples, crushed and sieved to the particle size under 2 mm, were placed in bidistilled water (high quality deionized water has a conductivity of about 0.5 μS/cm = 0.05 mS/m at 25°C) with a liquid volume (L)/solid weight (kg) ratio of 10:1 and maintained the vessel sealed for the entire duration of the test. Once the leaching test period (24 h at 25°C) was completed, the samples were taken out and cooled before being re-weighed to gauge the mass loss. The samples were filtered immediately using sterile 0.45 μm filters to ensure that there was no further equilibration between the powdered sample and the leachate, and also prevented any solid particulates from being introduced into the analytical system.

After the extraction and filtration of the leachate solution, heavy metal ions concentrations were determined employing a combination of Inductively Coupled Plasma Optical Emission Spectrometry (ICP-OES, Perkin-Elmer Optima 3000DV, United States) and Inductively Coupled Plasma Mass Spectrometry (ICPMS, Perkin-Elmer Elan 6,000, United States). Before ICP analysis, the samples were acidified with HNO<sub>3</sub> to pH = 2 to prevent any possible hydrolysis and precipitation of metal cations.

### Compressive Strength

The compressive strength of sample GP-MgO-rich was determined according to EN 196-1<sup>4</sup> using Toninorm equipment (Toni Technik, Germany; force application rate of

<sup>4</sup><http://www.euroslag.com/products/eaf/>.

0.05 kN/s). The reported strength measurement values represent the average results obtained from three test specimens of dimension (20 × 20 × 40) mm<sup>3</sup>. The compressive strength of GP-CaO-rich, GP-CaO-rich-BAS, GP-CaO-rich-NC, and GP-SW was similarly tested using parallelepiped geometry (40 × 40 × 80) mm<sup>3</sup> (according to ASTM C349 recommendation<sup>5</sup>) on an Instron machine. In this case, the compressive strength was also presented by the average of at least three specimens.

## Ecotoxicity Test on Consolidated Materials Antibacterial Activity

Antibacterial properties of synthesized GP-MgO-rich were evaluated against the Gram-negative *Escherichia coli* (American Type Culture Collection-ATCC 25922), and *Pseudomonas aeruginosa* (ATCC27853) and Gram-positive *Enterococcus faecalis* (ATCC 9212) in pellets. *E. coli* was grown on TBX Medium (Tryptone Bile X-Gluc), *P. aeruginosa* was cultured in *Pseudomonas* CN Agar (both provided by Liofilchem, Italy), while *E. faecalis* was grown in Slanetz-Bartley agar base (Liofilchem, Italy). For diluting bacteria pellets, autoclaved saline water (0.9% NaCl) was used. For the analysis of antibacterial properties of the sample, the following procedure was followed: sample was ground into a powder and then was weighted to obtain the different amount of GP-MgO-rich to place on Petri dishes. The powders were sterilized by UV light for 1 h. A pellet of bacterial strain (*E. coli*, *P. aeruginosa* and *E. faecalis* alternatively) was dissolved in 3.0 ml of autoclaved saline water obtaining a bacterial suspension of 10<sup>5</sup> CFU/ml. After plating the bacteria on its own medium, the samples were placed on the center of 6 cm in diameter of the plate. *E. coli* was incubated at 44°C for 24 h, while *P. aeruginosa* and *E. faecalis* were incubated at 36°C for 48 h, respectively. For *P. aeruginosa* it was investigated the effect of different amounts of GP-MgO-rich (5, 10, 25, 50, 100, 150 and 250 mg) while the effect of 50, 100, 150 and 250 mg were studied on *E. coli* and *E. faecalis*. The diameter of inhibition halos (IDs) in relation to Petri dish diameter (6 cm) were calculated. Four measures for each sample were carried out to determine the mean standard deviation.

Antimicrobial susceptibility test of GP-CaO-rich, GP-CaO-rich-BAS, GP-CaO-rich-NC, SW, and GP-SW samples was carried out to obtain preliminary information on antibacterial properties of these samples. *Escherichia coli* (ATCC 25922), Gram-negative bacteria and *Staphylococcus aureus* (ATCC 25923), Gram-positive bacteria were grown in the absence and presence of each sample. Samples used for analysis were radiated by UV light for 1 h to sterilized sterilize them. Two quantities of each grounded sample (100 and 200 mg) were tested. For GP-SW 100 mg of ground sample and a whole disk (500 mg) were used for this test. The bacterial suspension of 10<sup>5</sup> CFU/ml was obtained by diluting the strains in sterilized saline water (0.9% NaCl). *E. coli* was plated as reported above, while *S. aureus* on Baird-Parker agar (Liofilchem, Italy). Both media were sterilized up to 120°C for 15 min. After the sterilization process, Baird-Parker agar was cooled to 50°C and an emulsion of egg yolk containing

potassium tellurite was added. The samples were placed in the middle of Petri dishes. *E. coli* and *S. aureus* plates were incubated at 44 and 36°C, respectively, for 24 h. The diameter of inhibition halos (IDs) in relation to Petri dish diameter (DD) (6 cm) was calculated. Four measures for each sample were carried out to determine the mean standard deviation.

## Cytotoxicity Tests

Mouse embryonic fibroblast NIH-3T3 cell-line cells were cultured in Dulbecco's modified Eagle's medium (DMEM) supplemented with 10% Foetal Bovine Serum (FBS), containing penicillin and streptomycin antibiotics (100 µg/ml each) at 37°C in a humidified atmosphere containing 5% CO<sub>2</sub>. The cells were seeded in 6-mm well in the 96 Petri dish, and 24 h after been directly exposed to two doses of GP-MgO-rich (0.75 and 1.5 mg) and of GP-CaO-rich, GP-CaO-rich-BAS, GP-CaO-rich-NC, SW, and GP-SW samples (0.5 and 1.0 mg). After further 24 h of exposure time, the media was removed and replaced with fresh media containing 3-[4, 5-dimethylthiazol-2-yl]-2, 5-diphenyl tetrazolium bromide (MTT 0.5 mg/ml; Sigma Aldrich) at 37°C for 4 h. Then, this culture medium was removed and dimethylsulfoxide (DMSO) was added to the 96-well plates. The optical density of the solution was measured at the wavelength of 570 nm with a microplate reader (VictorIII Perkin Elmer, Waltham, MA, United States ) to release the coloured product into the solution. Representative cellular morphology images were acquired by Inverted phase Contrast Brightfield Zeiss Primo Vert microscope (Catauro et al., 2017). The MTT data are expressed as cell viability (CV, %) ± SD (standard deviation) of three independent measurements.

## RESULTS

### Chemical and Mechanical Stability Integrity

In order to evaluate the reticulation degree of the consolidated materials after the alkaline activation of the slags and stone wool powders, the integrity test was carried out. Visual inspection of all the formulations immersed in water for 24 h revealed no change in appearance or surface cracks or softening. Additionally, the liquid solution showed no color change or sediment formation. Yet, weight loss was recorded (Figure 2) for a maximum amount of around 11 wt% for GP-MgO-rich formulation. The three formulations based on CaO-rich slag recorded a loss of about 6–8 wt%, whilst the GP-SW formulation showed the most stable reticulation with only 2 wt%.

The good chemical performance in water was correlated to the measure of compressive strength (Figure 2). The highest value of the resistance to compression was measured for GP-MgO-rich, being the other four compositions in between 8 and 19 MPa.

### pH and Ionic Conductivity

The pH and ionic conductivity values provided significant information about the resistance of the reticulation into the alkali activated material after its contact with the aqueous environment.

<sup>5</sup>EN 196-1:2016-Methods of testing cement-Part 1: Determination of strength.

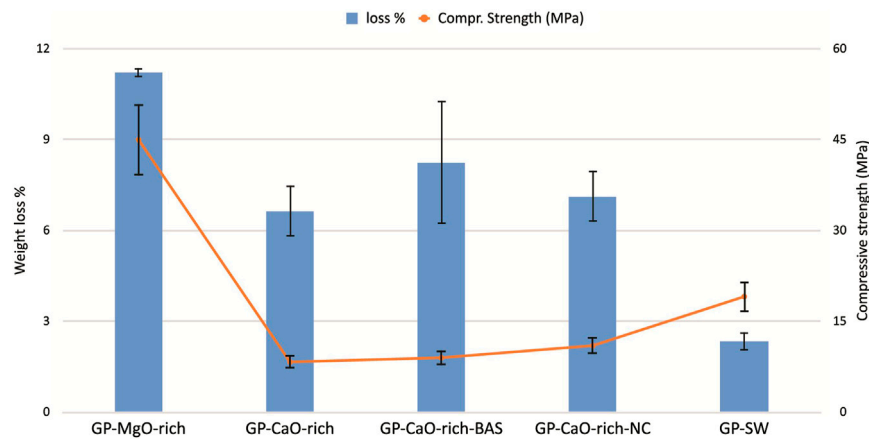


**FIGURE 2** | Weight Loss (%) and compressive strength (MPa) of the alkali activated materials.

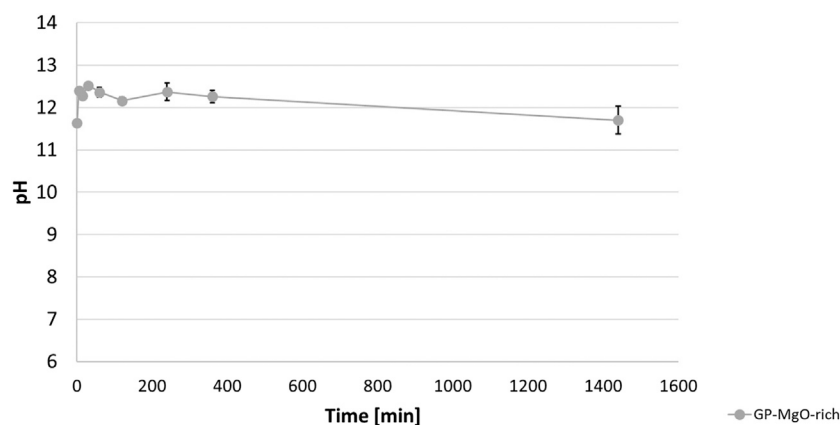


**FIGURE 3** | Monitoring the pH of water where a piece of sample GP-MgO-rich (S/L = 1:10) was immersed at room temperature.

The variation of the pH as a consequence of the immersion in fresh water of one piece (S/L = 1:10) of alkali activated material has been monitored overtime for the first 24 h. In **Figure 3** the pH measurement is reported, as an example, for the formulation GP-MgO-rich. Very similar trends are shown by the other formulations and are reported in **Supplementary Figure S1** (in the Supplementary Materials). How it can be observed in **Figure 3**, the variability of the sample is very reduced since the values of pH reported in the plot represent the average values of three repeated measures and error is the variance (approx. equal to 2%).

The variation of the ionic conductivity of the same leachate solution, with S/L = 1:10, was also monitored over the first 24 h of AAMs immersion. In **Figure 4** the ionic conductivity measurement is reported, as an example, again for the formulation GP-MgO-rich. Very similar trends are shown by the other formulations and are reported in **Supplementary Figure S2** (in the Supplementary Materials). Also in this case (**Figure 4**), the variability of the sample is very reduced since the values of ionic conductivity reported in the plot represent the average values of three repeated measures and error is the variance (approx. equal to 8%).

The pH and ionic conductivity values for all the compositions have been compared in **Figure 5**. These values were collected after the first 24 h of immersion when a constant value is reached.

The low values recorded for SW are due to its lack of wettability in water (as visible in **Supplementary Figure S3**), thus, in both cases, the values are those of the bidistilled water used for the tests.

Except for sample SW, all the formulations indicate a pH value between 11 and 12, accompanied by an ionic conductivity of the solution that shows a more irregular trend. In general, the AAMs exhibit higher ionic conductivity values with respect to the starting raw materials. The most evident effect is visible for GP-CaO-rich formulation where the addition of fillers increases 20% (basalt fibers) and 38% (nanocellulose) the values of ionic conductivity.

### Leaching Tests and Heavy Metal Release

In consideration of the fact that a solid matrix placed in the environment can see some mobile compounds biochemically altered and washed by the rains (elution or percolation), it is advisable to control these phenomena. Even more so if the

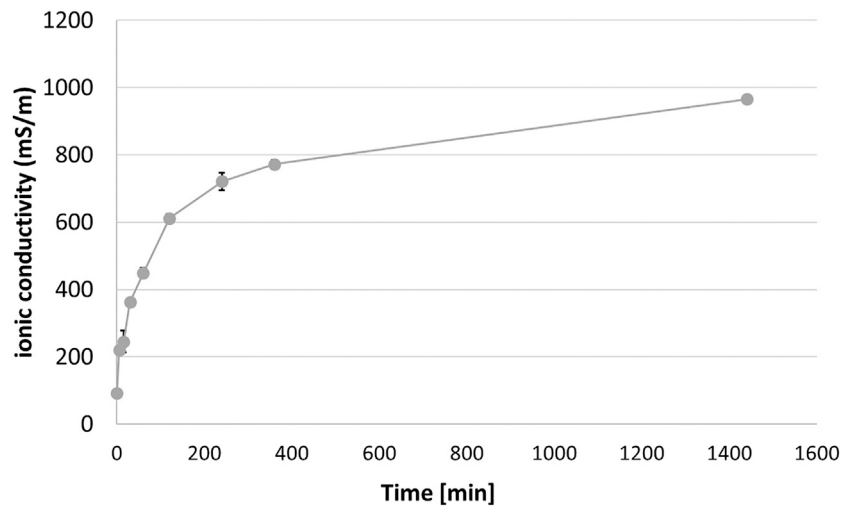


**FIGURE 4** | Monitoring the ionic conductivity (mS/m) of water where a piece of sample GP-SW (S/L = 1:10) was immersed at room temperature.

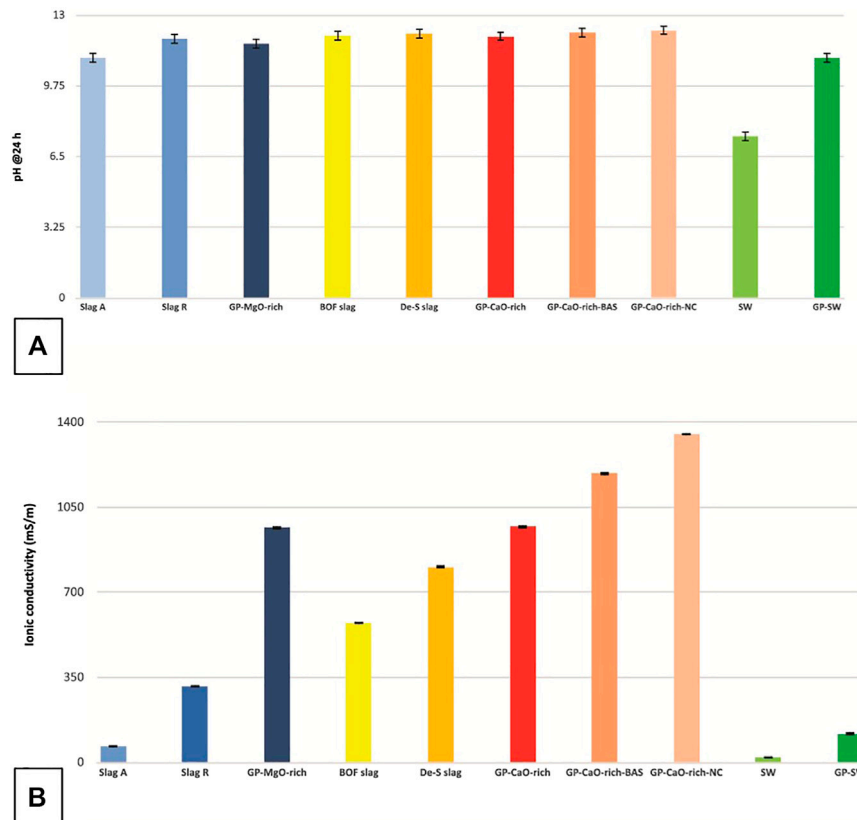


**FIGURE 5** | Value of pH (A) and ionic conductivity (mS/m) (B) of the leachate after 24 h' immersion in fresh water. Reference value is a geopolymer produced with metakaolin.

material contains residue or waste, it is necessary to proceed in this direction by adopting standardized and regulated methods, failing to accurately simulate the various scenarios with complex experiments, with sophisticated equipment and long-term

analyses. In all cases of land or waste classification according to legislation (EN 10802–2004 or EN 12457–2004) or for the assessment of potential emissions into the environment, the leaching agent used is always demineralized water which,

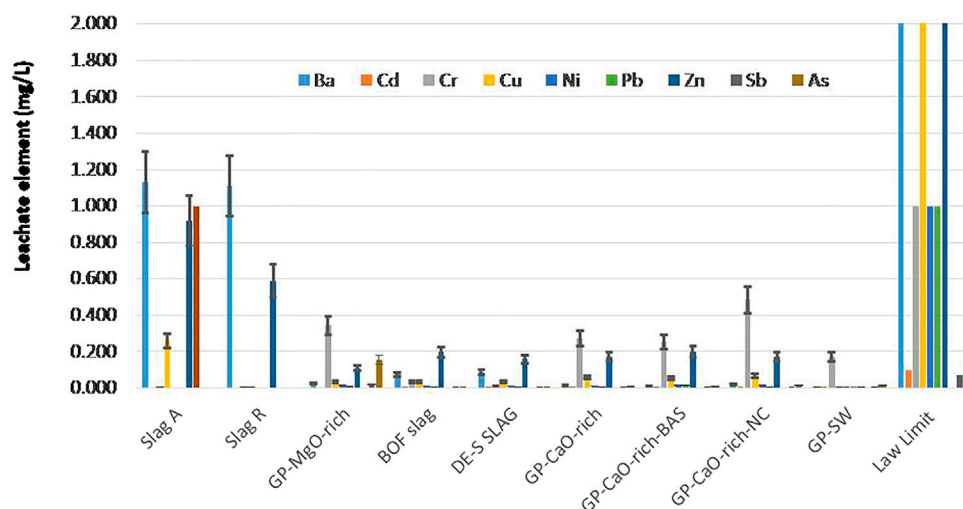


**FIGURE 6** | Comparison of the leachate elements from the starting slags and SW with the same element leachate out from the corresponding AAMs. Reference law limit values are taken from European Directive 1999/31/CE (<https://eur-lex.europa.eu/legal-content/EN/TXT/PDF/?uri=CELEX:31999L0031&from=PL>).

thanks to its polar nature, is able to consider a wide spectrum of species (polar compounds, elements in ionic form, some metals bound in mobile form, some organic molecules, etc.).

Within this research context, the analysis of the release of heavy metals in water verified the eventual hazardous nature of alkali activated materials and their immobilization efficiency.

**Figure 6** shows that all metals were less than the law limit (European Directive 1999/31/CE<sup>6</sup>), confirming the non-dangerous nature of raw materials and respective alkali activated materials. In particular, the slag A and slag R showed high values of Ba, Cu, and Ni, which decreased in their alkali activated material, GP-MgO-rich. This behavior confirmed the immobilization efficiency of the alkali activated materials comparing the amount of the leachable amount of the element from the geopolymer structure in water as already observed for alkali activated materials containing wastes (Kiventerä et al., 2018). GP-MgO-rich showed an increase of Mo according to literature (Lancellotti et al., 2021). The same immobilization behaviour characterized the other alkali activated materials, GP-CaO-rich, GP-CaO-rich-BAS, GP-CaO-rich-NC, except for Cr that increased after the alkaline activation, but it remained lower than the law limit. However, the literature demonstrates that the geopolymeric matrix increases the reticulation degree with time.

## Antibacterial Activity

The antibacterial properties of sample GP-MgO-rich have been investigated evaluating the growth of *Escherichia coli*, *Pseudomonas aeruginosa* and *Enterococcus faecalis* in the absence (sample indicated as Control in **Figure 7**) and the presence of an increasing amount of powder obtained from the consolidated final material. The inhibition halo is the empty area surrounding the central dark spot representing the geopolymeric powder. In **Figure 8** the dimension of these areas without bacterial growth has been measured (see Experimental

part) and reported for better evaluating the antibacterial effect of the specimen GP-MgO-rich. It can be noticed (**Figure 8**) that sample's powders do not a measurable halo for *P. aeruginosa* bacteria until the amount of 100 mg to the Petri Plate, thus being 50 mg the minimum amount necessary to have a quantification of the antibacterial efficiency in terms of measured halo. The inhibition halos for 150 and 250 mg samples are more visible (**Figure 8**). GP-MgO-rich exhibits an excellent antimicrobial activity against *E. coli*, in particular for 100–250 mg samples (**Figure 8**). In addition, it could be noticed that the size of the inhibition halo does not increase sensibly with the amount of powder above 100 mg, so we can conclude that GP-MgO-rich antibacterial activity does not depend on its quantity in this bacterial colony. Concerning *E. faecalis*, GP-MgO-rich formulation is not able to inhibit the bacterial growth for any of the amounts used for the experiment (**Figure 8**). Further, we have noticed that when 250 mg of powders are placed in the presence of bacteria, a slight inhibition halo is visible. This means that the poor antibacterial properties for this specific strain could be measured in presence of higher amounts. Nevertheless, it was possible to compare the effects of the same alkali activated material, GP-MgO-rich, with respect to the three strains, and it can be concluded that it presents a greater bacterial activity against *E. coli* with respect to other strains, as evidenced by the higher halo diameters for amount above 100 mg. The tests with the amounts of sample of 250 mg exhibit similar diameter dimensions for *P. aeruginosa* and *E. coli*.

For the antibacterial analysis of the other AAMs, we adopted only two different strains of bacteria, a Gram-negative (*E. coli*) and a Gram-positive (*S. aureus*). **Figure 9** represents the susceptibility test of *E. coli* and *S. aureus*, at two fixed amounts of alkali activated material, 100 and 200 mg. It can be noticed a general trend for the GP-CaO-rich AAMs: they can inhibit the growth of both bacteria tested, but seem to be more effective against Gram-negative than Gram-positive bacteria. For *E. coli* a slightly greater reduction of bacterial viability is observed

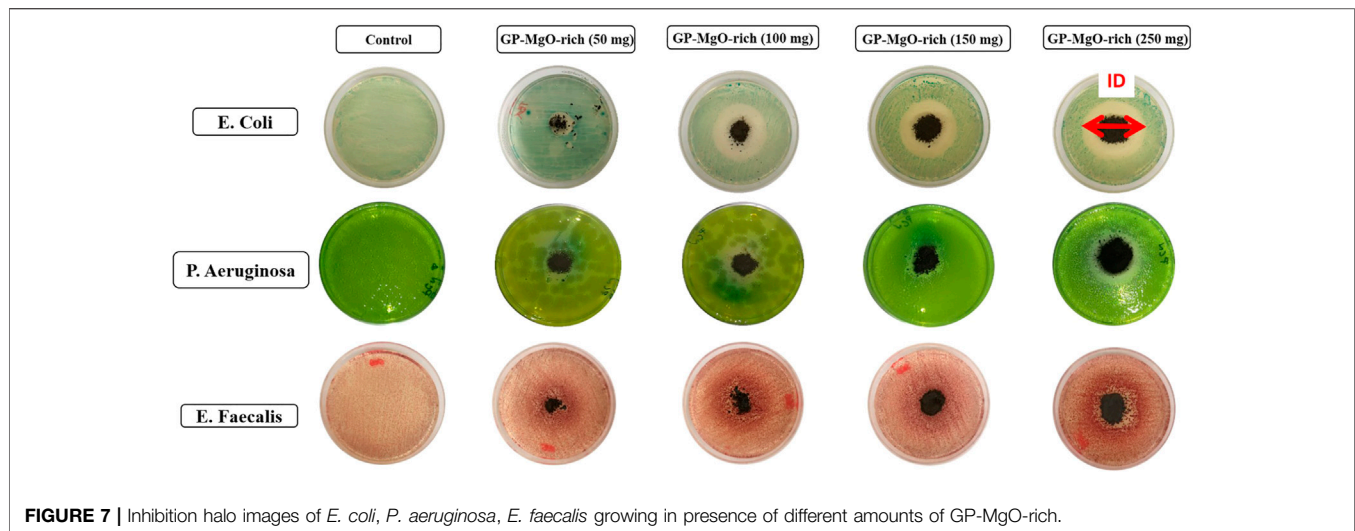


**FIGURE 7** | Inhibition halo images of *E. coli*, *P. aeruginosa*, *E. faecalis* growing in presence of different amounts of GP-MgO-rich.

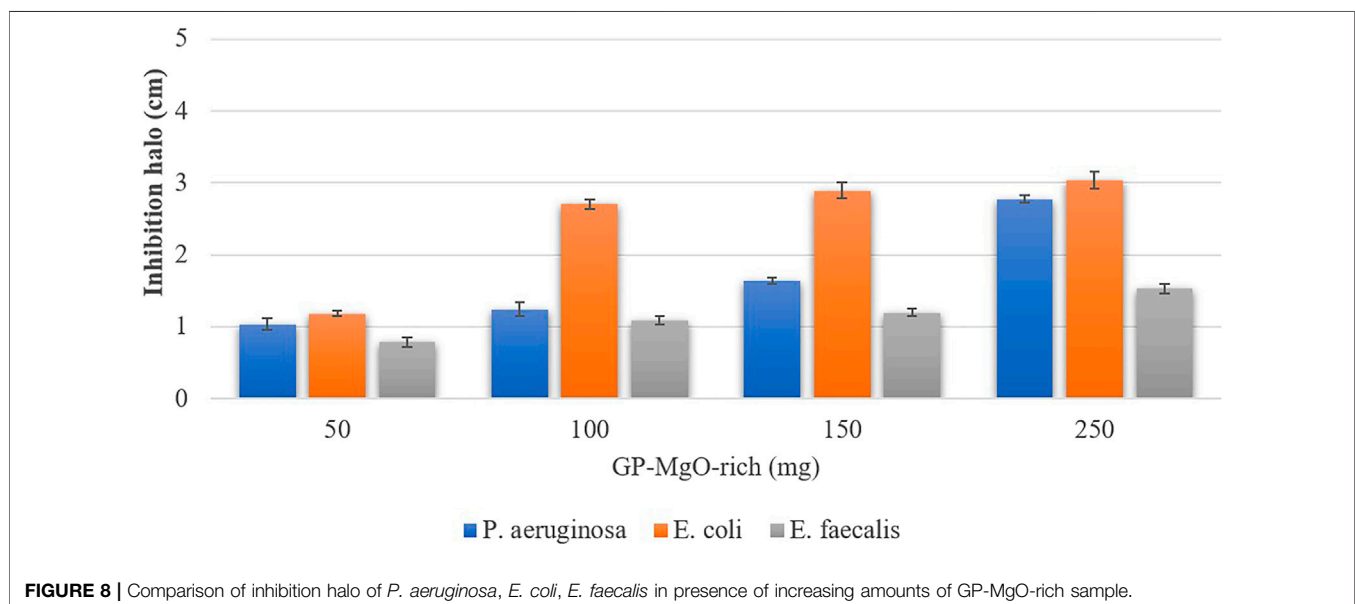


**FIGURE 8** | Comparison of inhibition halo of *P. aeruginosa*, *E. coli*, *E. faecalis* in presence of increasing amounts of GP-MgO-rich sample.

when quantities of samples are increased from 100 to 200 mg (Figure 9). This effect is also barely visible for *S. aureus* in presence of the two composites. No antibacterial properties are evident for stone wool and GP-SW for both bacteria tested. The GP-MgO-rich sample seems to be more effective because it shows a larger inhibition halo diameter when 100 mg are tested.

These results can also be expressed as Bacterial Viability-BV (in percentage) using the following formula:

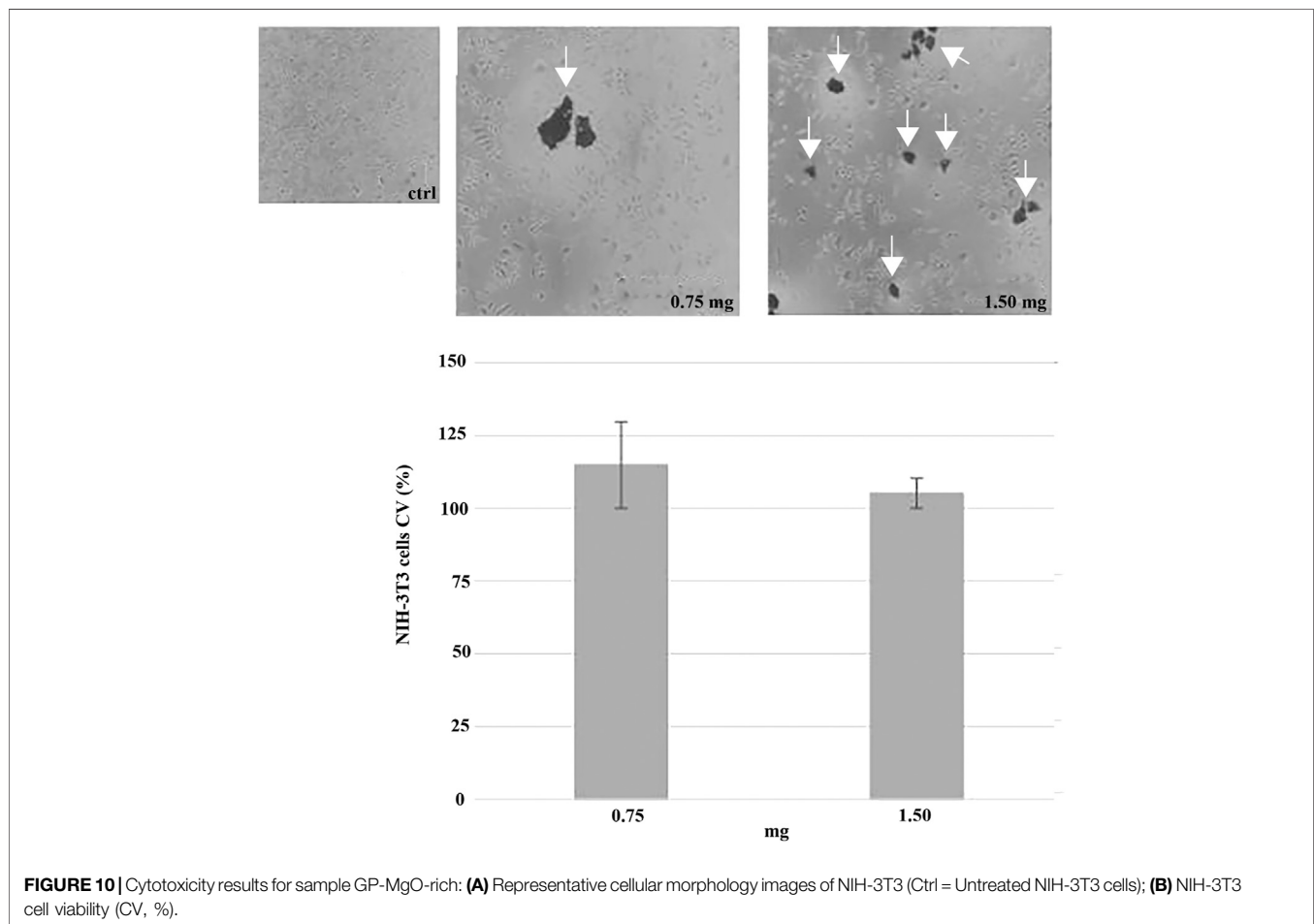
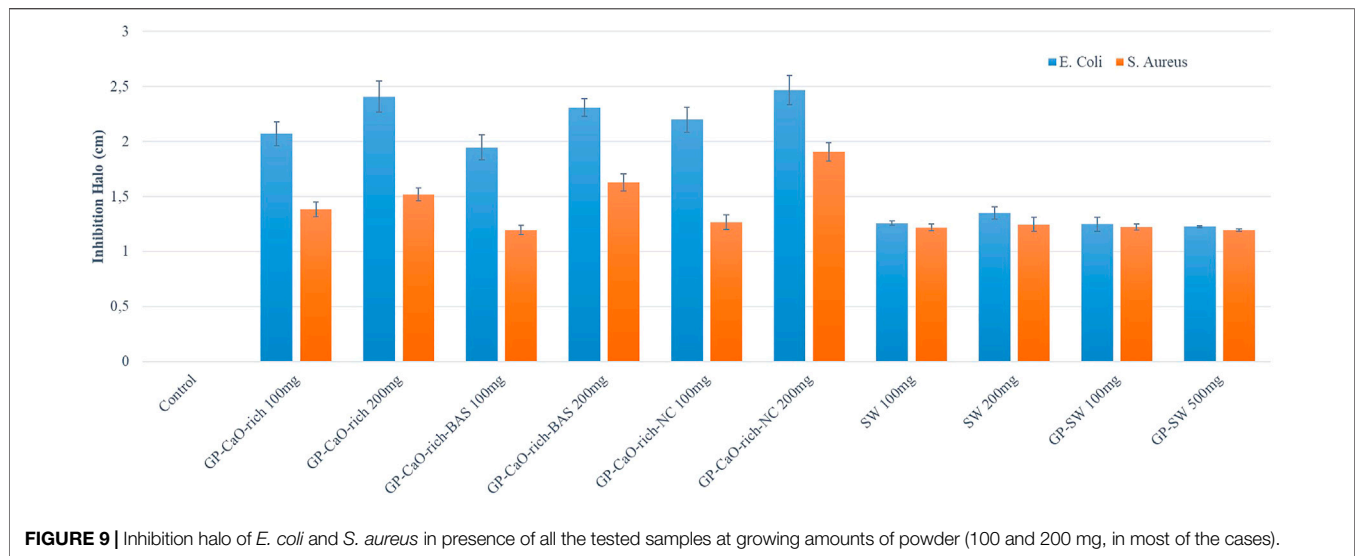
$$BV = [(DD - IDs) / (DD)] \times 100 \quad (2)$$

where IDs are the diameter of inhibition halos, DD is the Petri dish diameter, 6 cm for our experiments. Bacterial viability without samples is expressed as  $BV = 100\%$ . Referring to Figures 7–9, we observed a variability from  $BV = 80\%$  to  $BV = 50\%$ , the last value recorded only for GP-MgO-rich samples in the amount of 250 mg in presence of *P. aeruginosa* and *E. coli*, *E. faecalis*.

## Cytotoxicity

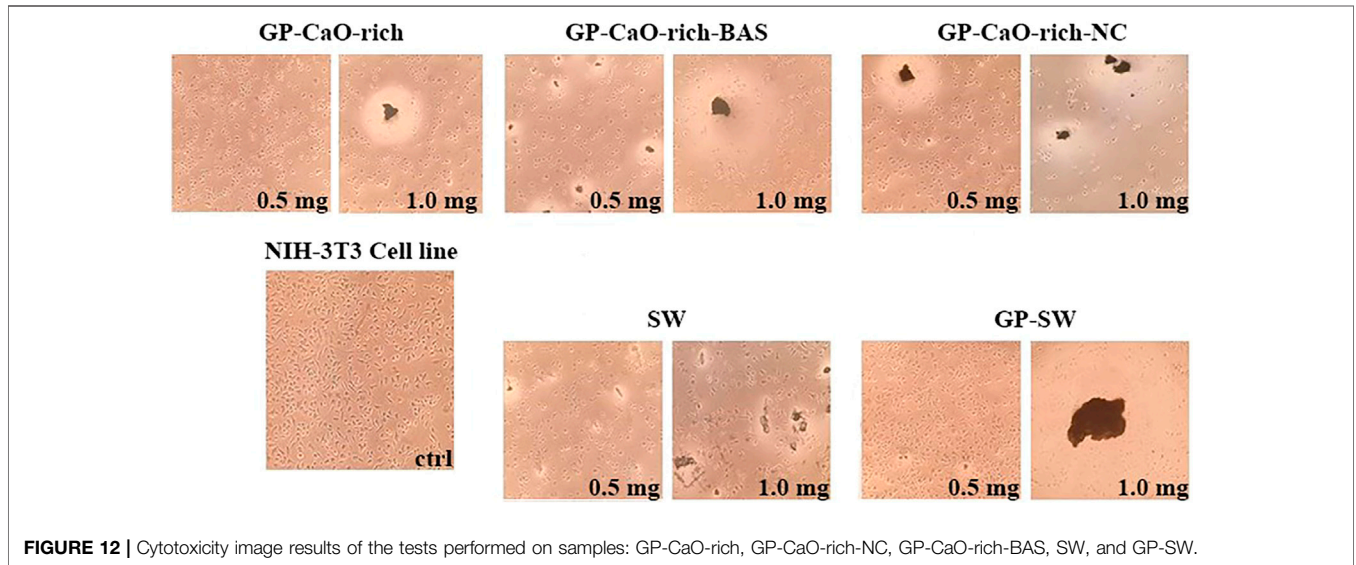
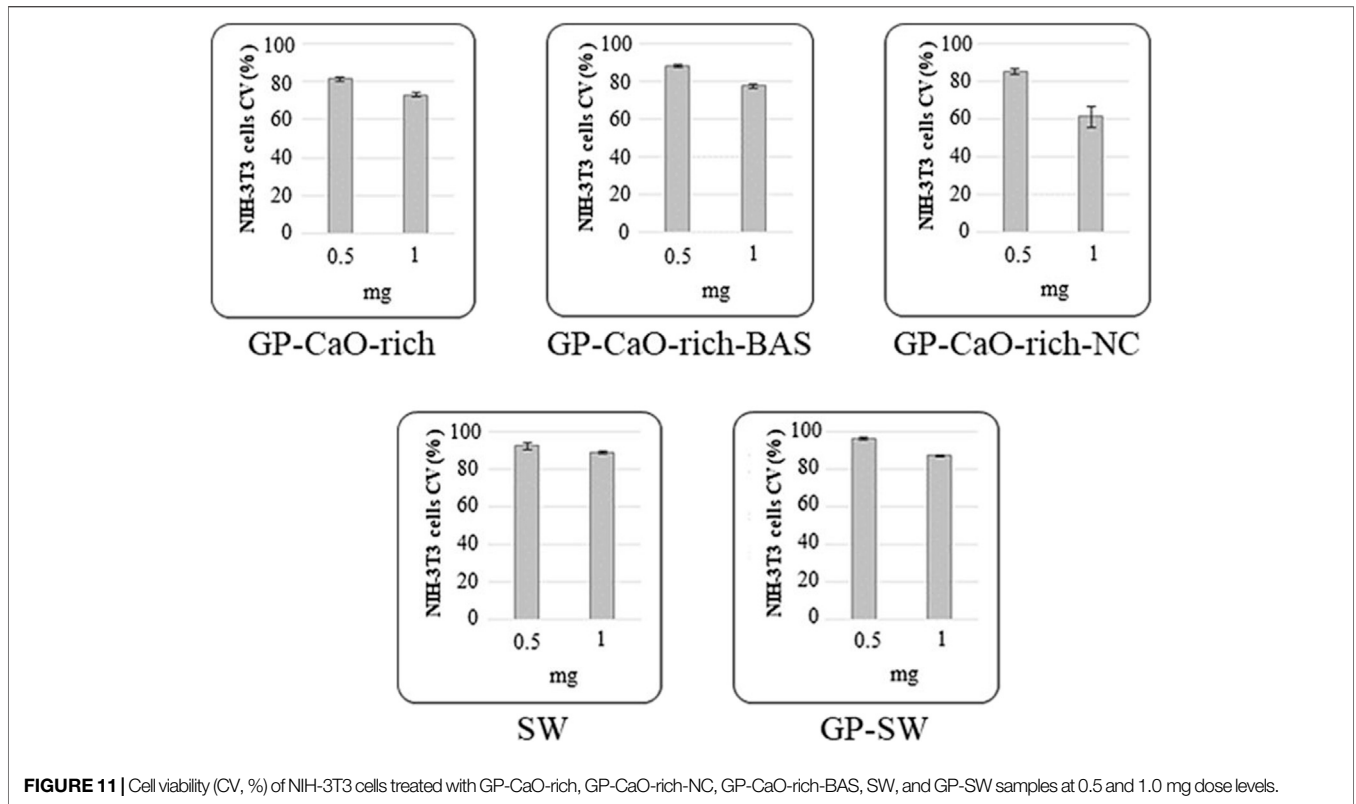
Cytotoxicity *in vitro* was evaluated on NIH-3T3 fibroblasts cell line placing GP-MgO-rich powders directly onto cells growing on culture medium, and MTT test was performed after 24 h' exposure time. Data acquired highlighted that GP-MgO-rich sample shows no apparent toxicity to NIH 3T3 cells. In particular, the results revealed that none of the doses used induced cell morphological changes (Figure 10A), and did not interfere with the mitochondrial metabolism, expressed as cell viability %, of the NIH 3T3 fibroblast cells (Figure 10B). Please notice that the CV parameter is typically 100% when negative effects are absent during regular cell growth.

The investigated samples were tested for their ability to modulate NIH-3T3 redox mitochondrial activity at different low exposure doses. For this purpose, a MTT direct test was performed. Formulation GP-CaO-rich and its two composite



samples appeared to be biocompatible when they were tested at 0.5 mg dose level (Figure 11). Indeed, an increase in the exposure dose favored an important cell viability decrease. This is particularly true for the GP-CaO-rich-NC sample, which was able, when directly exposed at the dose level 1.0 mg, to inhibit by

40% cell viability. NIH-3T3 cells appeared to be also morphologically compromised (Figure 12). SW and GP-SW samples did not negatively affect the cell viability. In fact, a  $\Delta RA$  (%) equal to 4% was calculated when the response of 0.5 and 1 mg SW samples were compared.



## DISCUSSION

### Alkali Activation and Properties of the Final Consolidated Materials

It has been already proved that in the case of alkali activation of metallurgical slags the hydraulic activity as well as the pozzolanic

activity increases as CaO, MgO, and Al<sub>2</sub>O<sub>3</sub> increase and SiO<sub>2</sub> and Al<sub>2</sub>O<sub>3</sub> increase, respectively (Oyebisi et al., 2020). In our case, the MgO-rich slags as well as the CaO-rich ones reacted well with the proper alkali media, belonging to the first class of slags. This means that the consolidation via the formation of the sodium activated gel typical of AAMs is combined with the hydraulic

phases, typical of Ordinary Portland Cement (OPC). These two phases (see also the next paragraph for details) co-exists and provide good chemical and mechanical stability to the final products (Garcia-Lodeiro et al., 2011).

The pH values of geopolymers after 24 h in water are in line with metakaolin-based geopolymers (pH = 10.9) with values around 11 (Figure 5). The trend is an initial increase and the reaching of a plateau for longer times. The value for metakaolin-based geopolymer is in line with Aly et al., showing pH = 10.5 (Aly et al., 2008). This specific work refers to the formulations capable of stabilizing nuclear wastes, thus offering the best chemical resistance and durability possible for a geopolymer formulation. The similarity of the measured pH values of our samples with those reported in this study allows us to be confident in a good durability of the consolidated products under investigation.

On the other hand, the behavior in terms of ionic conductivity is similar to the trend, but the values of metakaolin-based geopolymers are lower (203 mS/m) (Figure 5) (Sgarlata et al., 2021). This can be due to both the high amount of ions contained in crystalline phases which did not participate in the geopolymerization process thus after a long time they solubilize in water leaving the excessive amount of activation solution unreacted.

The pH values were constant during the monitoring time, in fact at 24 h all alkali activated materials showed pH under 12, according to the values of metakaolin-based geopolymers (pH of about 10.9). Instead, the alkali activated materials showed an increase of ionic conductivity with respect to their raw materials; in particular, GP-MgO-rich reached around 1,000 mS/m at 24 h compared to 100 mS/m of slag A and 300 mS/m of slag R. The same behaviour was confirmed by GP-CaO-rich, GP-CaO-rich-BAS and GP-CaO-rich-NC, which showed a higher value than BOF slag and De-S slag. An exception was observed by GP-SW that was characterized by a very low value of ionic conductivity with respect to other samples. This one showed a similar trend as in metakaolin-based geopolymers, in fact, it reached at 24 h a value of 200 mS/m, which confirms the consolidation of the polymeric network (Figure 5B).

The balance of the reactions giving rise to pH changes is complex and not very well understood. Pores' water transfer to the leachate increases pH, further, alkaline leachate attacks the unreacted constituents and the GP framework to form  $\text{Si}(\text{OH})_4$  monomer species in solution,  $\text{OH}^-$  ions, in this case, are consumed, causing a decrease of pH. The increase of conductivity with respect to the starting raw materials is due to the fact that the most leachable species in geopolymers are the  $\text{Na}^+$  ions from both pore water and the excessive amount of activating solution added (Aly et al., 2008).

The chemical stability is not directly proportional to the compressive strength (compare Figure 2 with Figure 5). The metakaolin-based geopolymers exhibit compressive strength around 38–45 MPa, in line with GP-MgO-rich and a little higher than GP-SW. The formulations with CaO-rich slags present very low values of mechanical strength whilst their chemical resistance is particularly good. These low values go along with those typical of non-structural materials, such as brick,

tiles and foamed panels for thermal insulation. Concerning dense materials, we can compare our results with those reported by Ozturk et al. (Ozturk et al., 2019) who studied activation of electric arc furnace slag with the mixture of sodium hydroxide and sodium silicate. The best-performance resulted mortar specimen reached compressive strength of 22.0 MPa. Turker et al. (Turker et al., 2016) on the other hand reached the maximum compressive strength of 40.7 MPa by activating slag with the same mixture of activators, which is also very comparable with the compressive strength of the GP-MgO-rich system in our study. Taking into account also the study from Santamaria-Vicario et al. (Santamaria-Vicario et al., 2016) who activated the mixture of electric arc furnace and ladle slag, resulting in the compressive strengths of 22.2 MPa, our results with these types of precursor exhibit good mechanical performance in comparison to other studies.

The mineralogical composition of GP-MgO-rich AAMs was already studied elsewhere (Češnovar et al., 2019a, Češnovar et al., 2019b). Crystal patterns of AAMs show the presence of numerous minerals (quartz, wustite, merwinite, chromite, perovskite, dolomite, calcite, ankerite, corundum, periclase, gehlenite, brucite, mayenite, and larnite) all deriving from one of the two precursors, either slag A or slag R. The mineral phases, however, are due to their crystalline nature, inert to the alkali-activation process and are thus present in XRD pattern of both precursors as well as in the hardened AAMs. The quantity of amorphous phase determined from Rietveld analysis was around 60 wt% in such systems and is presenting the immobilization matrix preventing heavy metals to be leached from the system.

In GP-CaO-rich AAMs, the phase assemblage included calcite (ca. 10–12 wt%), a trace of portlandite (ca. 9 wt%), and an amorphous fraction of ca. 50 wt%. Calcite formed as the carbonate after the carbonation of BOF slag, while the amorphous was likely C-S-H with a minor fraction of Al incorporated. In contrast, the stone wool based geopolymer formed a C-(N-)A-S-H gel and low-ordered Mg-Al LDH, as reported previously in (Nguyen et al., 2020; Yliniemi, et al., 2020).

It has been confirmed that both CSH gel as well as alkali activated gels could trap heavy metals inside their structure and prevent the leaching. Mechanism is complex and it depends on the type of gels (and the overall chemistry of investigated systems including activators) as well as on heavy metals cations. Alkali-activated slags contain higher amounts of gel pore compared to OPC and significantly lower amount of capillary pores which can play an essential role in their immobilization potential of heavy metals. In the study performed by Deja (Deja, 2002) immobilization of Zn, Cd, Cr, and Pb in alkali-activated slag were studied and it was found out that degree of  $\text{Cd}^{+2}$ ,  $\text{Zn}^{+2}$ , and  $\text{Pb}^{+2}$  immobilization was very high (over 99.9 %), while for  $\text{Cr}^{6+}$  was somewhat lower (ca. 99.0 %). For cesium, for example, which was investigated in the alkali activated blast furnace slag (Komljenovic et al., 2020) it was identified (by means of solid-state MAS-NMR) that it is preferentially associated with the alkali aluminosilicate gel rather than with the calcium aluminosilicate gel. The leaching behavior can be improved also by additional material with high sorption capacity, such as zeolite (Provis and

van Deventer, 2014), which might additionally extend the potential use of AAM for immobilization purposes.

In conclusions, the formation of different reacted gels such as calcium (sodium) aluminosilicate hydrate, C-(N)-A-S-H, and sodium aluminosilicate hydrate, N-A-S-H, gel (see discussion also in the next paragraph) can affect the mechanical properties of different AAMs developed in this study. In addition, the porosity of the confined materials likely plays a role influencing these properties. This aspect requires more thorough investigations as well as beyond the scopes of the present study.

## Leaching Behavior and Ecotoxicity

The condensed phases of alkali activated materials containing a high amount of CaO, such as the slags under investigations, have been deeply investigated by several groups (White et al., 2015). At atomic scale investigations using X-ray pair distribution function analysis, the atomic and nanostructure of alkali-activated cement gels have revealed an intrinsic difference with Ordinary Portland Cement (OPC) phases, based mainly on tricalcium silicate (C3S), known as the basic component of clinker.

It has been proved that the calcium silicate hydrate (C-S-H) gel, with a Ca/Si ratio of 1.7 (Allen et al., 2007), and calcium aluminosilicate hydrate (C-A-S-H) gels derived from C3S pastes are nanocrystalline in nature, being extended up to ~40 Å, i.e. the particle size of the gel grains.

Alkali-activated slag binders, or cements, due to the large percentage of calcium present an atomic bonding environment of a calcium (–sodium) aluminosilicate hydrate (C-(N)-A-S-H) gel very similar to that observed in OPC-based cements (Puertas et al., 2011). Such C-(N)-A-S-H gel in alkali-activated slag paste was accurately studied with synchrotron diffraction of XRD and the pair-distribution function indicated that it is predominantly amorphous because it only contains coherent atom–atom correlations up to ~15 Å (White et al., 2015). This information on the extension of the newly formed 3D C-(N)-A-S-H gel during the alkali activation process of slags, indicates that most of the slag particles remain unreacted in the paste. Therefore, we evaluated the leaching behavior of the slags and stone wool in water before and after the alkali activation, so as to evidence the chemical stability created by the formation of the C-(N)-A-S-H amorphous gel.

Our results of the leaching in water (Figure 6) indicate a very limited release of toxic heavy metals from part of the AAMs that we investigated. The eventual toxic effects of the presence of these heavy metal cations in aqueous solutions were tested either for bacteria as well as for cells.

GP-MgO-rich exhibits a good antimicrobial, reaching the lower value of BV = 50%, against *E. coli*, a bacterium characterized by different pathogenic behavior, responsible for many common bacterial infections and persistent in various environments (van Elsas et al., 2011), in particular for the amount of samples corresponding to 100–250 mg. In our study, we evaluated the antibacterial activity of the geopolymers, assaying directly the solid materials on Petri's dishes where the bacteria were plated. When the materials are placed on the agar, the pH of the agar becomes alkaline and it could be difficult to carry the heavy metals to the bacteria.

Nevertheless, the bacteria very close to the materials undergo membrane leakage pouring out the cytoplasmic environment, typically at about pH 7, thus locally reducing the alkalinity and increasing the solubility of heavy-metal hydroxides. The combination of both the slow increment of the pH and the presence of heavy metals affect the bacterial growth. According to Erdoğrul and Erbilir (Erdoğrul and Erbilir, 2005) *E. coli* is able to adapt to alkaline pH, which efforts the ability of that strain to activate the genes responsible for the proteins involved into alkaline environment survival (Saito and Kobayashi, 2003). The combination of the alkali stress and the increase of pH affects negatively the bacterial viability of *E. coli*, leading to an increase of the inhibition halos visible in Figure 7. The occurrence of these contemporary phenomena is less visible on Petri's plate where *E. faecalis* and *P. aeruginosa* were grown. The former is tolerant for alkaline pH values (Flahaut, et al., 1997), while the latter possesses a good heavy-metal resistance (Nies, 1999). Indeed, no increase of halo diameters, for *P. aeruginosa* plates, above 100 mg was observed, so it can be concluded that antibacterial activity does not depend on sample's the amount.

As regards GP-CaO-rich AAMs, they can inhibit the growth of both bacteria tested, but seem to be more effective against Gram-negative than Gram-positive bacteria, indeed for *E. coli* a slightly greater reduction of bacterial viability is observed for high quantities of samples 200 mg, while this effect is also barely visible for *S. aureus* which is a pathogen of greatest concern because of its resistance to common antibiotics and it can cause life-threatening infections (Lowy, 2003).

No antibacterial properties are evident for stone wool and GP-SW for both bacteria tested, BV > 95%.

Regarding the cytotoxicity experimental evidences, GP-MgO-rich sample shows no apparent toxicity to NIH 3T3 cells in terms of both cell morphological changes and interferences with the mitochondrial metabolism. The formulation GP-CaO-rich and its two composite samples appeared to be biocompatible, when they were tested at 0.5 mg dose level. Indeed, an increase in the exposure dose favored an important cell viability decrease. This is particularly true for the GP-CaO-rich-NC sample to inhibit by 40% CV and induce morphological changes. SW and GP-SW samples did not negatively affect cell viability.

The results of the antibacterial and cytotoxicity tests can be correlated with the leaching test. GP-CaO-rich-NC presents the higher release of chromium with respect to the other compositions, while the other two GP-CaO-rich compositions have higher values of Cu and Zn. GP-MgO-rich presents significant chromium release even if below the law limit and a corresponding excellent antimicrobial activity against *E. coli*.

Stone wool compositions, that have neither weight loss or release of metals, did not negatively affect cell viability and do not show any antibacterial properties.

The analysis of the leachate reveals the presence of divalent cations such as Cu and Zn. These can interact with the membranes of bacteria and enter the cytoplasm. These cations can then modify the activities of normal life by inducing cell death (ROS, homeostasis negative influence on the enzymes) (Nies, 1999). The absence of these cations and a basic pH value, as in

OPC-Ordinary Portland Cement, does not lead to any effect, except for a light color change in the dye used to evident the bacterial culture (**Supplementary Figure S4** in Supplementary Materials). In our cases, the cytotoxicity test was evaluated toward mouse embryonic fibroblast cells, indicating that the heavy metals contents in the leachate for all samples were not toxic to cells (Popovich et al., 2020; Catauro et al., 2020; Sutanto et al., 2020; Catauro et al., 2021).

## CONCLUSION

In the slag-based AAMs, the molecular “zeolite-like” structures and bonding of alkali-activated gels are responsible for the aluminosilicate network stability as well as for the macroscopic degradation phenomena, and are thus also affecting the environmental impact on living organisms and cells. The high percentage of amorphous phase (50–60%) was likely due calcium (sodium) aluminosilicate hydrate, C-(N-)-A-S-H, and sodium aluminosilicate hydrate, N-A-S-H, gel. Such a high amount of gel implicates a likewise amount of gel pores and significantly lower amount of capillary pores which can play an essential role in their immobilization potential of heavy metals. The leaching tests indicated that the heavy cation release in water was contained below regulation limits and slightly affected the biological environment, either bacteria or cellular cultures.

From this study, it was concluded that GP-MgO-rich AAMs exhibit a good antimicrobial activity against *E. coli* with respect to other strains for amounts above 100 mg. Further, a general trend for the GP-CaO-rich AAMs was observed, which were more effective against Gram-negative than Gram-positive bacteria. To add, almost no antibacterial properties were evident for stone wool and GP-SW for both bacteria tested, BV = 95–100%. Further, the GP-MgO-rich sample also shows no apparent toxicity to NIH 3T3 cells. In particular, the results revealed that none of the doses used induced cell morphological changes, and did not interfere with the mitochondrial metabolism. The results of the antibacterial and cytotoxicity can be correlated with the leaching test. GP-CaO-rich-NC presents the higher release of chromium with respect to the other compositions, while the other two GP-CaO-rich compositions have higher values of Cu and Zn. GP-MgO-rich presents significant chromium release even if below the law limit

## REFERENCES

- Allen, A. J., Thomas, J. J., and Jennings, H. M. (2007). Composition and Density of Nanoscale Calcium-Silicate-Hydrate in Cement. *Nat. Mater.* 6, 311–316. doi:10.1038/nmat1871
- Aly, Z., Vance, E. R., Perera, D. S., Hanna, J. V., Griffith, C. S., Davis, J., et al. (2008). Aqueous Leachability of Metakaolin-Based Geopolymers with Molar Ratios of Si/Al=1.5–4. *J. Nucl. Mater.* 378, 172–179. doi:10.1016/j.jnucmat.2008.06.015
- Benassi, L., Alias, C., Feretti, D., Gelatti, U., Piovani, G., Zerbini, I., et al. (2019). Ecotoxicity and Genotoxicity of Steel Slags: Preliminary Results. *Detritus* 2019, 1–38. doi:10.31025/2611-4135/2019.13815
- Catauro, M., Barrino, F., Pacifico, S., Piccolella, S., Lancellotti, I., and Leonelli, C. (2021). Synthesis of WEEE-Based Geopolymers and Their Cytotoxicity. *Mater. Today Proc.* 34, 121–124. doi:10.1016/j.matpr.2020.01.408

and a corresponding excellent antimicrobial activity against *E. coli*.

With this study we evidenced the absence of ecotoxicity in terms of heavy cation release and in terms of bio-impact, this study will help to convince the citizen that there are viable alternatives to OPC-based concrete that can greatly reduce CO<sub>2</sub> consumption in building practices.

## DATA AVAILABILITY STATEMENT

The original contributions presented in the study are included in the article/**Supplementary Material**, further inquiries can be directed to the corresponding author.

## AUTHOR CONTRIBUTIONS

IL, JY, VD and CL conceived and supervised the research. CS, FP, GDP, and MC designed the experiments. FP, GDP, MC, KT, and HN performed the experiments. IL, MC, and CL analyzed the experimental results. All authors participated in writing and editing the article.

## FUNDING

This research was supported by funds from the ERA-MIN two Project « FLOW-Lightweight alkali activated composite foams based on secondary raw materials » Project No. C 3330-18-252010, <http://flow.zag.si/en>.

## ACKNOWLEDGMENTS

Authors are particularly grateful to Gregorio Vaccari for the preparation of the figures.

## SUPPLEMENTARY MATERIAL

The Supplementary Material for this article can be found online at: <https://www.frontiersin.org/articles/10.3389/fmats.2021.689290/full#supplementary-material>

- Catauro, M., Lancellotti, I., and Leonelli, C. (2017). Addition of WEEE Glass to Metakaolin-Based Geopolymeric Binder: A Cytotoxicity Study. *Environments* 4, 89. doi:10.3390/environments4040089
- Češnovar, M., Traven, K., Horvat, B., and Ducman, V. (2019b). The Potential of Ladle Slag and Electric Arc Furnace Slag Use in Synthesizing Alkali Activated Materials; the Influence of Curing on Mechanical Properties. *Materials (Basel)* 12, 1173. doi:10.3390/ma12071173
- Češnovar, M., Traven, K., and Ducman, V. (2019a). “Alkali Activated Foams from Slag (FLOW),” in Proceedings of the 6th International Slag Valorisation Symposium (Leuven, Belgium: KU Leuven), 1–5. Available at: <https://slag-valorisation-symposium.eu/2019/>.
- Deja, J. (2002). Immobilization of Cr<sup>6+</sup>, Cd<sup>2+</sup>, Zn<sup>2+</sup> and Pb<sup>2+</sup> in Alkali-Activated Slag Binders. *Cement Concrete Res.* 32 (12), 1971–1979. doi:10.1016/S0008-8846(02)00904-3

- Erdoğrul, Ö., and Erbilir, F. (2005). Resistance of *Escherichia coli* to Acid and Alkali pH. *Ann. Microbiol.* 55 (2), 91–95.
- Flahaut, S., Hartke, A., Giard, J. C., and Auffray, Y. (1997). Alkaline Stress Response in *Enterococcus faecalis*: Adaptation, cross-protection, and Changes in Protein Synthesis. *Appl. Environ. Microbiol. Environ. Microbiol.* 63 (2), 812–814. doi:10.1128/AEM.63.2.812-814.1997
- García-Lodeiro, I., Palomo, A., Fernández-Jiménez, A., and MacPhee, D. E. (2011). Compatibility Studies between N-A-S-H and C-A-S-H Gels. Study in the Ternary Diagram  $\text{Na}^2\text{O}-\text{CaO}-\text{Al}^2\text{O}^3-\text{SiO}^2-\text{H}^2\text{O}$ . *Cement Concrete Res.* 41, 923–931. doi:10.1016/j.cemconres.2011.05.006
- Jiang, Y., Ling, T.-C., Shi, C., and Pan, S.-Y. (2018). Characteristics of Steel Slags and Their Use in Cement and concrete-A Review. *Resour. Conservation Recycling* 136, 187–197. doi:10.1016/j.resconrec.2018.04.023
- Kinnunen, P., Yliniemi, J., Talling, B., and Illikainen, M. (2017). Rockwool Waste in Fly Ash Geopolymer Composites. *J. Mater. Cycles Waste Manag.* 19, 1220–1227. doi:10.1007/s10163-016-0514-z
- Kiventerä, J., Lancellotti, I., Catauro, M., Poggetto, F. D., Leonelli, C., and Illikainen, M. (2018). Alkali Activation as New Option for Gold Mine Tailings Inertization. *J. Clean. Prod.* 187, 76–84. doi:10.1016/j.jclepro.2018.03.182
- Komljenović, M., Tanasijević, G., Džunuzović, N., and Provis, J. L. (2020). Immobilization of Cesium with Alkali-Activated Blast Furnace Slag. *J. Hazard. Mater.* 388, 121765. doi:10.1016/j.jhazmat.2019.121765
- Lancellotti, I., Piccolo, F., Traven, K., Češnovar, M., Ducman, V., and Leonelli, C. (2021). Alkali Activation of Metallurgical Slags: Reactivity, Chemical Behavior, and Environmental Assessment. *Materials* 14, 639. doi:10.3390/ma14030639
- Lowy, F. D. (2003). Antimicrobial Resistance: the Example of *Staphylococcus aureus*. *J. Clin. Invest.* 111, 1265–1273. doi:10.1172/jci20031853510.1172/jci18535
- Ly, L., Vance, E. R., Perera, D. S., Aly, Z., and Olufson, K. (2007). Leaching of Geopolymers in Deionised Water. *Azoojomo* 3. doi:10.2240/azoojomo0238
- Mastali, M., Shaad, K. M., Abdollahnejad, Z., Falah, M., Kinnunen, P., and Illikainen, M. (2020). Towards Sustainable Bricks Made with Fiber-Reinforced Alkali-Activated Desulfurization Slag Mortars Incorporating Carbonated Basic Oxygen Furnace Aggregates. *Constr. Build. Mater.* 232, 117258. doi:10.1016/j.conbuildmat.2019.117258
- Nguyen, H., Kaas, A., Kinnunen, P., Carvelli, V., Monticelli, C., Yliniemi, J., et al. (2020). Fiber Reinforced Alkali-Activated Stone Wool Composites Fabricated by Hot-Pressing Technique. *Mater. Des.* 186, 108315. doi:10.1016/j.matdes.2019.108315
- Nies, D. H. (1999). Microbial Heavy-Metal Resistance. *Appl. Microbiol. Biotechnol.* 51, 730–750. doi:10.1007/s002530051457
- Oyebisi, S., Ede, A., Olutoge, F., and Olukanni, D. (2020). Assessment of Activity Moduli and Acidic Resistance of Slag-Based Geopolymer concrete Incorporating Pozzolan. *Case Stud. Construction Mater.* 13, e00394. doi:10.1016/j.cscm.2020.e00394
- Ozturk, M., Bankir, M. B., Bolukbasi, O. S., and Sevim, U. K. (2019). Alkali Activation of Electric Arc Furnace Slag: Mechanical Properties and Micro Analyzes. *J. Building Eng.* 21, 97–105. doi:10.1016/j.jobee.2018.10.005
- Popovich, J., Chen, S., Iannuzzo, N., Ganser, C., Seo, D.-K., and Haydel, S. E. (2020). Synthesized Geopolymers Adsorb Bacterial Proteins, Toxins, and Cells. *Front. Bioeng. Biotechnol.* 8, 1–12. doi:10.3389/fbioe.2020.00527
- Provis, J. L., and van Deventer, J. S. J. (2014). Alkali-Activated Materials; State-Of-The-Art Report. Available at: [https://www.rilem.net/global/gene/link.php?doc\\_id=3969&fg=1](https://www.rilem.net/global/gene/link.php?doc_id=3969&fg=1) (Accessed June 29, 2021).
- Puertas, F., Palacios, M., Manzano, H., Dolado, J. S., Rico, A., and Rodríguez, J. (2011). A Model for the C-A-S-H Gel Formed in Alkali-Activated Slag Cements. *J. Eur. Ceram. Soc.* 31, 2043–2056. doi:10.1016/j.jeurceramsoc.2011.04.036
- Rowles, M., and O'Connor, B. (2003). Chemical Optimisation of the Compressive Strength of Aluminosilicate Geopolymers Synthesised by Sodium Silicate Activation of Metakaolinite. *J. Mater. Chem.* 13, 1161–1165. doi:10.1039/b212629j
- Rubio-Avalos, J.-C. (2018). Antibacterial Metakaolin-Based Geopolymer Cement. *RILEM Bookseries* 16, 398–403. doi:10.1007/978-94-024-1207-9\_64
- Saito, H., and Kobayashi, H. (2003). Bacterial Responses to Alkaline Stress. *Sci. Prog.* 86 (Pt 4), 271–282. doi:10.3184/003685003783238635
- Santamaría-Vicario, I., Rodríguez, A., Junco, C., Gutiérrez-González, S., and Calderón, V. (2016). Durability Behavior of Steelmaking Slag Masonry Mortars. *Mater. Des.* 97, 307–315. doi:10.1016/j.matdes.2016.02.080
- Setién, J., Hernández, D., and González, J. J. (2009). Characterization of Ladle Furnace Basic Slag for Use as a Construction Material. *Construction Building Mater.* 23, 1788–1794. doi:10.1016/j.conbuildmat.2008.10.003
- Sgarlata, C., Formia, A., Ferrari, F., and Leonelli, C. (2021). Effect of the Introduction of Reactive Fillers and Metakaolin in Waste Clay-Based Materials for Geopolymerization Processes. *Molecules* 26 (5), 1325. doi:10.3390/molecules10.3390/molecules26051325
- Sutanto, D., Satari, M. H., Hernowo, B. S., Priosoeryanto, B. P., Septawendar, R., Asri, L. A. T. W., et al. (2020). Geopolymer-carbonated Apatite Nanocomposites with Magnesium and Strontium Trace Elements for Dental Restorative Materials. *J. Korean Ceram. Soc.* 57, 546–556. doi:10.1007/s43207-020-00060-x
- Türker, H. T., Balçikanlı, M., Durmuş, İ. H., Özbay, E., and Erdemir, M. (2016). Microstructural Alteration of Alkali Activated Slag Mortars Depend on Exposed High Temperature Level. *Construction Building Mater.* 104, 169–180. doi:10.1016/j.conbuildmat.2015.12.070
- van Elsas, J. D., Semenov, A. V., Costa, R., and Trevors, J. T. (2011). Survival of *Escherichia coli* in the Environment: Fundamental and Public Health Aspects. *ISME J.* 5 (2), 173–183. doi:10.1038/ismej.2010.80
- Väntsi, O., and Kärki, T. (2014). Mineral Wool Waste in Europe: A Review of mineral Wool Waste Quantity, Quality, and Current Recycling Methods. *J. Mater. Cycles Waste Manag.* 16, 62–72. doi:10.1007/s10163-013-0170-5
- White, C. E., Daemen, L. L., Hartl, M., and Page, K. (2015). Intrinsic Differences in Atomic Ordering of Calcium (Alumino)silicate Hydrates in Conventional and Alkali-Activated Cements. *Cement Concrete Res.* 67, 66–73. doi:10.1016/j.cemconres.2014.08.006
- Yliniemi, J., Kinnunen, P., Karinkanta, P., and Illikainen, M. (2016). Utilization of mineral Wools as Alkali-Activated Material Precursor. *Materials* 9, 312. doi:10.3390/ma9050312
- Yliniemi, J., Walkley, B., Provis, J. L., Kinnunen, P., and Illikainen, M. (2020). Nanostructural Evolution of Alkali-Activated mineral Wools. *Cement and Concrete Composites* 106, 103472. doi:10.1016/j.cemconcomp.2019.103472

**Conflict of Interest:** The authors declare that the research was conducted in the absence of any commercial or financial relationships that could be construed as a potential conflict of interest.

Copyright © 2021 Sgarlata, Dal Poggetto, Piccolo, Catauro, Traven, Češnovar, Nguyen, Yliniemi, Barbieri, Ducman, Lancellotti and Leonelli. This is an open-access article distributed under the terms of the Creative Commons Attribution License (CC BY). The use, distribution or reproduction in other forums is permitted, provided the original author(s) and the copyright owner(s) are credited and that the original publication in this journal is cited, in accordance with accepted academic practice. No use, distribution or reproduction is permitted which does not comply with these terms.